Impedance spectroscopy characterisation of automotive NMC/graphite Li-ion cells aged with realistic PHEV load profile

Quantification of cell properties *vs*. temperature at different stages of ageing

Ylva Olofsson, Jens Groot
Electromobility Sub-systems
Volvo GTT, Advanced Technology & Research
SE-412 88 Göteborg, Sweden
ylva.olofsson@volvo.com

Tomaž Katrašnik, Gregor Tavčar
Faculty of Mechanical Engineering
University of Ljubljana
Aškerčeva 6, SI-1000, Ljubljana, Slovenia

***Abstract*—The ageing behaviour of Li-ion cells in automotive applications is known to be strongly non-linear with respect to operating conditions. In addition, it has a profound impact on performance, cost and reliability of the target vehicle. The work presented in this paper concerns automotive type NMC/graphite Li-ion battery cells aged under realistic and accelerated conditions, analyzed using electrochemical impedance spectroscopy and with the implementation of an electric equivalent circuit model. Two cycle life tests were performed at +22°C and +45°C surrounding temperature, with reference performance tests performed at ±0°C, +22°C and +45°C. The duty cycle applied is derived from speed samples of real-world city driving characteristics for electric passenger cars with fast charging at 2C-rate. Results show that despite a significant decrease in capacity, a decrease in charge transfer resistance can be observed during the first stages of aging which may be correlated to an increased double layer capacitance. Also, an increase in peak power at low temperatures is observed.**

Keywords—Electrochemical impedance spectroscopy; Li-ion battery, LMO/NMC; cycle life test; accelerated ageing; electric equivalent circuit; duty cycle, electric vehicle

I. INTRODUCTION

Battery electric vehicles (BEVs) and hybrid-electric vehicles (HEVs) are already established on the marked with predicted significant market share increases in the future. Li-ion cells are the most widespread energy storage technology for this type of vehicles both in the short- to mid-term. In addition, at present it is well known that the battery pack often accounts for the highest cost, features the highest weight and largest volume among powertrain components, whereas it is also generally most prone to ageing and also one of the most safety critical components. It is thus of utmost importance to operate battery pack as close to optimum as possible to efficiently addressed aforementioned issues.

978-1-4799-6075-0/14/$31.00 ©2014 IEEE

This can on one hand be achieved by proper battery pack design and control, whereas on the other hand this is only possible if battery cells are well characterized in terms of cause and effect phenomena for a wide range of operating parameters including battery ageing.

It is well accepted that different types of Li-ion cells respond differently to the same stimuli, *e.g.* [1], therefore findings are not necessarily transferable between different types of Li-ion cells.

This paper focuses on identification of battery parameters with electrochemical impedance spectroscopy (EIS) at different states of battery ageing. The paper reports on a reduction of the charge transfer resistance during ageing similar to what has been already shown in [2] and in part reported by [10].

The innovative contributions of this paper can be summarized as: a) a series production LG Chem 41 Ah LMO/NMC cathode, Carbon/Graphite anode cell was analyzed according to a duty cycle reconstructed from the real-world drive cycle characteristic for electric vehicles; and b) reduced charge transfer resistance during ageing from beginning of life (BOL) towards middle of life (MOL) was correlated with the increased double layer capacitance.

II. EXPERIMENTAL METHOD

The experimental set- up is based on accelerated life cycle test at constant temperature applying a duty cycle with high currents and high energy throughput, and with DC and EIS reference measurements at ±0°C, +22°C and +45°C. The battery cell evaluated is a Li-ion LMO/NMC cathode, Carbon/Graphite anode 41 Ah cell, see properties in TABLE I.

A. Accelerated life cycle test

In order to reduce the time needed for the evaluation of aging effects, the measurements are commonly accelerated by applying a driving cycle of high stress and with peak currents of fast charging, and/or operated at elevated temperatures. The testing in this paper is performed during 3 months or until the

battery cell capacity is degraded to 80% of initial capacity, a level often used as end-of-life (EOL) criteria in vehicle applications. Cycle life tests were performed at two surrounding air temperatures; +22°C and +45°C. At strategic points during the cycle life test an extraction of parameters representing the electro-chemical cell properties is made at various SOC (state-of-charge) levels, temperatures and frequencies in order to relate the degradation and SOH (state-of-health) to different stress factors. These so called reference tests or check-ups are accomplished regularly according to an experimental sequence outlined in Fig. 1 in which the cell performance in terms of power, capacity, impedance and energy is measured.

TABLE I. CELL PROPERTIES AT +25°C ACCORDING TO SUPPLIER

Manufacturer	LG Chem
Application	PHEV, EV
Shape	Prismatic
Chemical characteristics	LMO/NMC cathode, Carbon/Graphite anode
Nominal capacity [Ah]	41
Nominal voltage [V]	3.75
Voltage range [V]	3 - 4.15
Energy density [Wh/kg]	159

Generally, the number of reference tests in a cycle life test should be low enough to avoid additional stress caused by the characterization itself, but still provide sufficient performance data to allow adequate evaluation of ageing effects. Consequently, full reference performance tests (FPC) were run at selected stages of cell ageing; beginning-of-life (BOL), middle-of-life (MOL), end-of-life (EOL) with partial performance tests (PPC) at intermediate steps. Here, MOL is arbitrarily defined as the point when the cell has lost approx. 10% of the initial capacity at 1C-rate. Complementary to Fig. 1, the temperatures for the different tests are displayed in TABLE II. The SOC levels for FPC and PPC are [0:10:100]% and [20:20:80]% respectively.

All test procedures are based on established test standards and experience from previous projects such as [3], [4], [5], [6] and [7] as well as internal projects. Formation, cycling, PPC and FPC tests are performed using a Maccor® battery tester and the EIS using a Gamry® potentiostat.

B. *Load cycle*

A load profile of charge depleting character is used to simulate the application in a BEV or PHEV passenger car city driving (Fig. 2- Fig. 3) and is run for 3 months in intervals of 196 load cycles between reference tests. Every discharge cycle is followed by a constant current charge of 2C up to 90% SOC. Adjustment of the SOC level at start of cycling is done regularly as the capacity fades to keep the cell cycling in a SOC window of 90-30 %. Details of the battery cell cycling characteristics are presented in TABLE III.

C. *Electrochemical impedance spectroscopy*

In addition to the FPC/PPC tests, electrochemical impedance spectroscopy (EIS) is applied to enable a more thorough assessment ageing in terms of changes in kinetic and mass transport parameters. Moreover, EIS allows for a simple translation of the physical system into an equivalent circuit model.

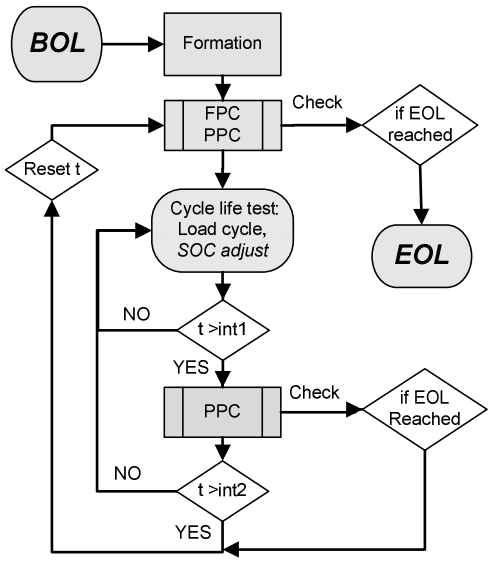

Fig. 1. Flowchart of test sequence plan from BOL to EOL including formation, PPC, FPC, and cycle life test. MOL is defined as 6 weeks completed cycling. Time int1= 2 weeks, int2 =4 weeks. See TABLE II. for related temperatures.

TABLE II. THE TEMPERATURES (°C) APPLIED FOR TESTS IN EXPERIMENTAL SET-UP (FIG. 1)

	BOL	*MOL*	*EOL*	*Intermediate*
FPC	22 & 45	22	22 & 45	-
PPC	0	0	0	22
Cycling	22/45	22/45	22/45	22/45

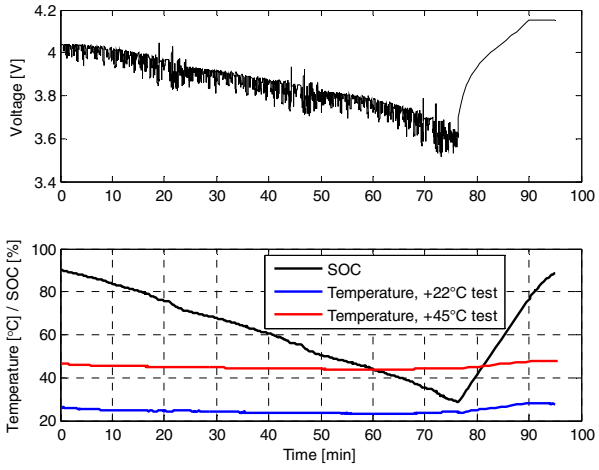

Fig. 2. Typical cell voltage, cell temperature and SOC during one load cycle followed by 2C charge up to 90 % SOC. A temperature rise of approx. 5°C is observed during the 2C charge step for the cell cycled at +22°C and a 4°C rise is observed for the cell cycled at +45°C.

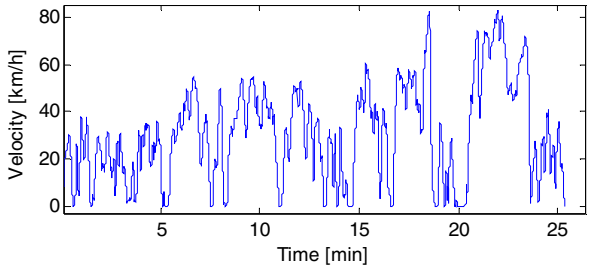

Fig. 3. Vehicle velocity in the "*Unsteady Long*" cycle previously presented in [7]. The velocity profile is used in multiples for a defined SOC window and translated to single cell load.

TABLE III. CYCLING PARAMETERS AND CYCLE CONDITIONS AT BOL

Max SOC [%]	90
Min SOC [%]	33
SOC window [%]	57
Voltage at start of cycle [V]	4.07
Voltage at end of cycle [V]	3.55
Cell voltage range [V]	3.00-4.15
Discharge energy [Wh]	94
Discharge capacity [Ah]	25
Peak charge current [A]	122
Peak discharge current [A]	-126
Peak charge current [C]	3.0
Peak discharge current [C]	3.1
Battery nominal capacity [Ah]	41
Ambient temperature [°C]	+22/+45
Average cell temperature during cycling [°C]	+25/+45
Minimum cell temperature during cycling [°C]	+23/+44
Maximum cell temperature during cycling [°C]	+28/+48
Cycle duration [min]	75

The EIS measurements are performed at 10 SOC levels in a C/2 multi-step galvanostatic sequence where each charge step is followed by a 15min rest period and a potentiostatic EIS sweep at 10mV AC, 0A DC, 100kHz-4mHz and 11 points / decade.

III. ELECTRIC EQUIVALENT CIRCUIT MODEL

Naturally, an electric equivalent circuit (EEC) model can be tailored to any level of complexity and resolution of internal battery parameters. Due to the limited set of cell properties given by the manufacturer, two relatively simple EECs were used for interpretation of results (Fig. 4). Despite their simplicity they proved to produce a relatively good fit to the measured EIS data in terms of stability, tolerance and relative error.

The different parameters are as follows presented in relation to the equivalent circuit model in Fig. 4 and to the *Nyquist* graphs in the results, section IV.

R_Ω: Ohmic Impedance. An approximate value can be obtained from the intersection between the impedance curve and the real axis. The ohmic impedance represents sum of the ohmic solution resistance in the electrolyte and all non-electrochemically active parts of the cell (electrical resistance in electrodes, current collectors, terminals etc.) and is expected to be comparably stable during battery ageing [2].

R_{CT}: Charge Transfer Impedance. The sum of this parameter and R_{SEI} below is approximately equal to diameter of the semi-circle of the impedance curve. R_{CT} represents the resistance in the charge transfer occurring at the electrode surface [2] and is often attributed to the *Butler-Volmer* kinetics of the reaction.

R_{SEI}: Solid electrolyte interphase (SEI) film impedance, representing the resistance to the transport of the charged species across the SEI film [9]. In many cases, R_{SEI} is too small to be distinguished from the larger R_{CT}. Hence, a simplified EEC can be used (Fig. 4).

C_{DL}: Double layer capacitance. The C_{DL} is modelled as a Constant Phase Element, (CPE) with a dispersion constant α_{DL} for precise model adjustment (1). The double layer is a region featuring a significant electric field between the electrode and the electrolyte acting like a capacitor [2]. Although the physical interpretation of the CPE is debated [11], its application and merits in empirical EECs are well-known.

C_{SEI}: Solid electrolyte interface (SEI) film capacitance, modelled as a CPE with a dispersion constant α_{SEI}. The SEI film represents a dielectric region acting like a capacitor [9].

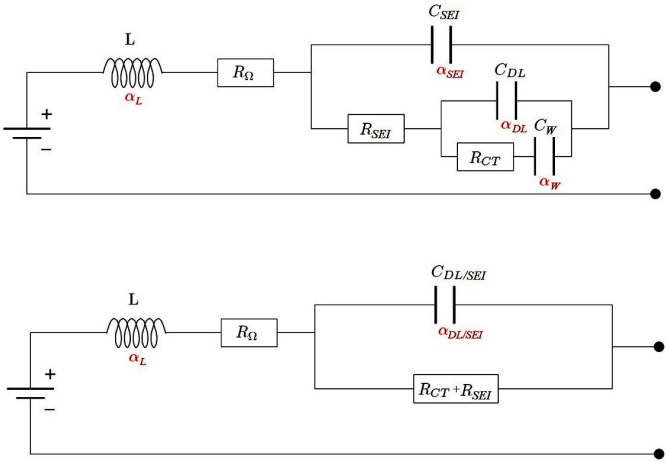

Fig. 4. Equivalent circuit models used for the modelling of measured EIS data. Top circuit used for modelling EIS behaviour at +0°C, bottom circuit used for modelling EIS behaviour at +22°C. In the later case the C_{SEI} and C_{DL} are modelled as a single effective capacitance.

C_w: Warburg impedance representing the capacitive impedance at low frequencies related to mass transport, similarly to the capacitances modelled as a CPE [2].

L: Inductance. The cell and of the conductors are taken into account by this parameter. A constant α_L is used in order to adapt the model for measurement equipment (2). In theory the inductive part of a prismatic single cell should be very small. Nevertheless, mutual inductance of cell leads, cables and instrument inaccuracies will, in most cases dealing with large-format cells and high current rates, result in a curved shape of the inductive impedance curve [2]. Consequently, the addition of the constant α_L may result in a significantly better and more stable fit. Furthermore, the discussion in this paper solely focuses on lower frequencies.

$$Z_{CPE} = ((j\omega)^{\alpha} C)^{-1} \qquad 0 < \alpha < 1 \qquad (1)$$

$$Z_L = (j\omega)^{\alpha} L \qquad 0 < \alpha < 1 \qquad (2)$$

IV. Results

From a vehicle point of view, the battery performance at low to medium temperature is most critical. Hence, the results presented in this section focus at the impedance at ±0°C and +22°C.

For comparability of results of cells aged at different temperatures the cell characterizations were performed at predefined set of age points defined by the number of cycles performed up to such a point. Thus, the MOL was defined as the characterisation point approximately corresponding to a 10% loss of capacity; at 610 cycles 8% loss of C/1-capacity was measured for the cell cycled at +22°C and 14% loss was measured for the cell cycled at +45°C (Fig. 5 and TABLE IV).

In the course of the testing only the cell aged at +45°C reached EOL (after 810 cycles), therefore only BOL and MOL characterizations are shown for +22°C and all three (BOL, MOL and EOL) for +45°C.

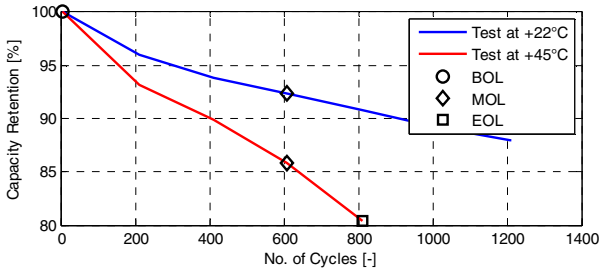

Fig. 5. Capacity retention *vs*. number of cycles for the two cycle life tests at +22°C and +45°C.

Both cells showed very similar performance at BOL, indicating high uniformity in cell manufacturing and, in turn, relatively reliable cycle life performance despite the lack of a large test matrix with several replicate tests.

Firstly, considering that the cell aged at +45°C reached the end of life after merely 810 cycles, this must be regarded as a sign of a relatively fast ageing, a severely accelerated load profile or a combination of the two. Not surprisingly the cell aged at +22°C degrades at a lower rate, however, considering that it takes only 600 cycles to reach 8% loss of capacity this should still be regarded as an accelerated ageing test.

Secondly, and in contrast to the often reported impedance growth correlated to the capacity decrease, the *Nyquist* plots of EIS impedance in Fig. 6 to Fig. 7 show a notable decrease of the semicircle diameter when comparing the MOL results to the BOL results, whereas Fig. 8 and Fig. 9 show that this trend does not continue when moving from MOL to EOL but rather a slight increase is observed. Additionally, it can be noted that the distance between the complex plane origin and the point where the *Nyquist* plot intersects the real axis increases with aging. Results for the ±0°C temperature feature an irregularly shaped semicircle. The equivalent circuit used for modelling the ±0°C data features two RC pairs (top circuit in Fig. 4): a high frequency one distinguished as a smaller arc on the left side of the distorted semicircle and a medium frequency one distinguished in the main arch of the distorted semicircle. In the case of the +22°C data, only one RC pair is used for modelling (bottom circuit in Fig. 4), since individual contributions of two distinct RC pairs are indistinguishable in such case. All this is reflected in the parameters of the equivalent circuit reported in TABLE IV. The equivalent circuit parameters also reveal significant changes in the related capacitances when comparing the three age points.

Lastly, the 10s-power at charge and discharge is not notably different at MOL compared to BOL, except for ±0°C where the cell maximum charge power is considerably better at MOL compared to BOL. This is well correlated to the lower impedance (Fig. 7), but may also be due to other factors such as faster self-heating or that the cell at BOL was not fully electrochemically activated.

It shall, however, also be pointed out that the average over-potential for complete charge and discharge with constant current is principally larger at MOL. Hence, despite a higher power capability and lower pulse impedance, the overall power efficiency of the cell is lower after partial ageing when complete charge/discharge cycles are considered.

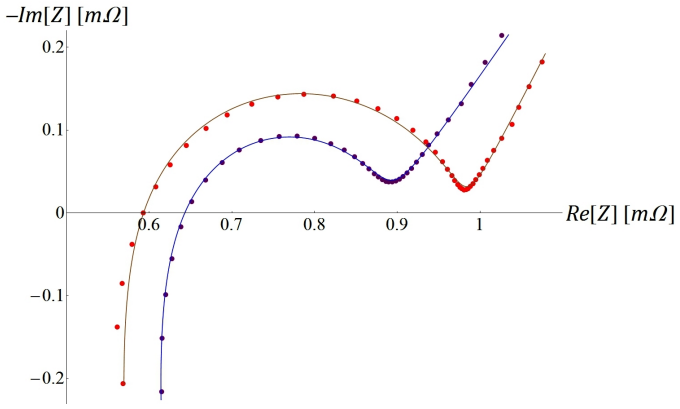

Fig. 6. *Nyquist* impedance plot of the cell aged at +22°C measured at +22°C, with red and blue points representing the BOL and MOL data respectively and the solid curves representing the respective equivalent circuit model response.

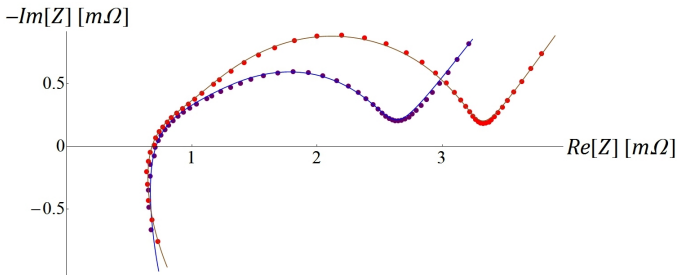

Fig. 7. *Nyquist* impedance plot of the cell aged at +22°C measured at ±0°C, with red and blue points representing the BOL and MOL data respectively and the solid curves representing the respective equivalent circuit model response.

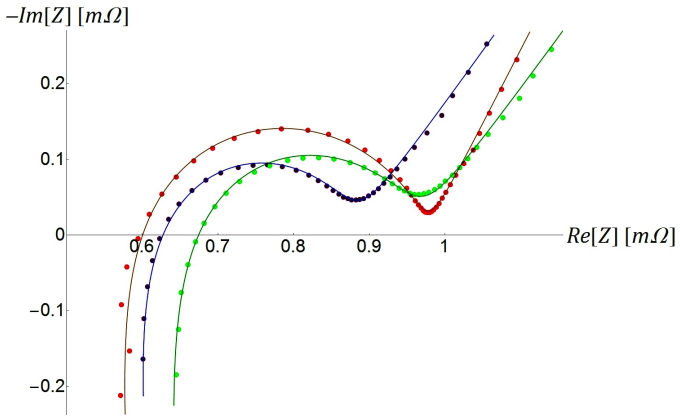

Fig. 8. *Nyquist* impedance plot of the cell aged at +45°C measured at +22°C, with red, blue and green points representing the BOL, MOL and EOL data respectively and solid curves representing the respective equivalent circuit model responses.

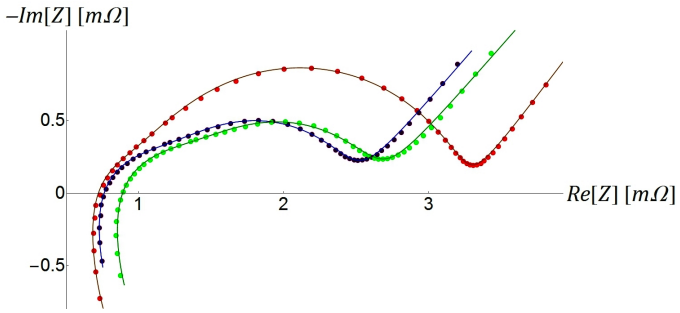

Fig. 9. *Nyquist* impedance plot of the cell aged at +45°C measured at ±0°C, with red, blue and green points representing the BOL, MOL and EOL data respectively and the solid curves representing the respective equivalent circuit model response.

V. Discussion

A distinct increasing of ohmic resistance with aging is observed in TABLE IV (R_Ω *fit*) and also in Fig. 6 to Fig. 7 (deduced from the real axis intersection). This phenomenon can be ascribed to electrolyte degradation and deterioration of the electro conductive contact between electrode constituents.

Other aging trends are not as monotonic as the change in ohmic resistance, thus it is worth splitting the aging analysis into two stages: the first stage being the aging from BOL to MOL (applicable to both cases, *i.e.*: aging at temperatures +22°C and +45°C) and the second stage being the aging from MOL to EOL (applicable only to the case of aging at +45°C). The first stage of aging is most notably characterized by a significant reduction of charge transfer resistance, with the following reasoning: The diameter of the semi-circle in the *Nyquist* curve is assumed to be the sum of the SEI film resistance and the charge transfer resistance. Whereas the measurements at +22°C only indicate a decrease of the combined resistance the measurements at ±0°C further reveal that the R_{CT} is the most likely candidate for the cause of this decrease. The concurrent decrease of the charge transfer resistance and the increase of the double layer capacitance as reported in TABLE IV indicate that one possible physical explanation may be an increased active surface area. In other words, the cell experiences an increase of the total interfacial area between the electrolyte and the solid electrode. Such increase should lead to both larger exchange current densities – and thus to a lower electron transfer resistance – and to a larger double layer capacitance as a direct consequence.

The experimental results at ±0°C also indicate that the resistance of the SEI film increases at MOL which can be explained with SEI film growth, a trend commonly reported in many publications, *e.g.* [9]. As reasoned in [9] the SEI film growth has also a detrimental effect to the rate of charge transfer reactions, which could explain why the decrease in charge transfer resistance is not as large as the increase in the double layer capacitance.

The second stage is to large extent characterized by a continuously increasing ohmic and SEI film resistance and insignificant changes of other parameters. This reasoning is supported primarily by an analysis of the equivalent circuit parameters at MOL and EOL of the +45°C aging case measured at ±0°C (TABLE IV.). Here, the values of charge transfer resistance and double layer capacitance appear to be stabilised, which would, in line with the above proposed explanation, mean that the active surface area increase only to a certain maximum value during aging. On the other hand, the SEI film resistance appears to grow continuously likewise to the ohmic resistance.

TABLE IV. BEGINNING-OF-LIFE (BOL), MIDDLE-OF –LIFE (MOL) AND END-OF-LIFE (EOL) CELL CHARACTERISTICS AT ±0°C AND +22°C.

Ageing Temperature	Measurement temperature	Age point	*C/1 Discharge Capacity [Ah]*	*Charge Power, 10s, 50% SOC [W]*	*Discharge Power 10s, 50% SOC [W]*	R_Ω *fit [mΩ]*	R_{CT} *fit [mΩ]*	R_{SEI} *fit [mΩ]*	C_{DL} *fit [F]*	C_{SEI} *fit [F]*	C_W *fit [kF]*
+22°C	**+22°C**	**BOL**	40.47 / 100%	808.1	-723.7	0.528	0.443		69.7		13.31
+22°C	**+22°C**	**MOL**	37.38 / 92%	794.8	-722.9	0.564	0.320		138.1		9.66
+22°C	**±0°C**	**BOL**	37.41 / 92%	376.7[1]	-652.4[1]	0.565	2.22	0.500	94.8	50.5	12.29
+22°C	**±0°C**	**MOL**	35.00 / 86%	408.0	-658.3	0.600	1.42	0.580	162.5	75.8	8.57
+45°C	**+22°C**	**BOL**	40.60 / 100%	807.7	-721.4	0.530	0.447		71.0		47.31
+45°C	**+22°C**	**MOL**	34.84 / 86%	785.0	-722.4	0.550	0.330		138.2		22.66
+45°C	**+22°C**	**EOL**	32.64 / 80%	730.2	-719.6	0.585	0.380		140.3		20.09
+45°C	**±0°C**	**BOL**	37.24 / 92%	373.4	-651.9	0.605	2.20	0.45	95.0	53.0	24.22
+45°C	**±0°C**	**MOL**	32.84 / 81%	402.9	-654.7	0.650	1.18	0.65	209.7	53.0	12.95
+45°C	**±0°C**	**EOL**	30.07 / 74%	347.6	-627.3	0.765	1.18	0.70	214.5	50.1	12.20

1. Average from 5 cells at BOL

The aging mechanism behind the increased active/interfacial area may be the consequence of micro-cracking of the solid granular electrode caused by the cyclic stress and strain during the operation. Thus this mechanism seems to lead to a higher porosity of the electrode(s).

Although the decreased electron transfer resistance at MOL and EOL is beneficial to the battery performance the overall battery performance (*i.e.* lower over-potential at charging and discharging) is better at BOL. The latter could primarily be attributed to the larger charge transport resistances.

In summary, the tested cells do not show monotonically changing characteristics when represented by equivalent circuits and EIS. Furthermore, there are significantly different ageing trends for different circuit parameters, and differences in ageing rates at the two studied temperatures. Since battery management units used to continuously monitor battery performance at internal states often rely on equivalent circuit models, the presented complexity of the ageing trends must be considered to achieve a robust performance of such control systems.

VI. ACKNOWLEDGEMENTS

The present work is a part of the project ASTERICS GA No 314157, co-funded by the 7th Framework Programme of the EC – European Commission DG Research:
http://cordis.europa.eu/fp7/cooperation/home_en.html
http://ec.europa.eu
http://www.asterics.eu

The publication as provided reflects only the author's view.

REFERENCES

[1] W. Prochazka, G. Pregartner and M. Cifraina, "*Design-of-Experiment and Statistical Modeling of a Large Scale Aging Experiment for Two Popular Lithium Ion Cell Chemistries*", Journal of The Electrochemical Society, April 2013, 160 (8), pp. A1039-A1051.

[2] J. Groot, "*State-of-health estimation of li-ion batteries: Cycle life test methods*" *Chalmers University of Technology, Göteborg* (2012).

[3] EUCAR- (European Council for Automotive R&D), is an industrial association making R&D within mobility and transport in efficiency, safety, environmental, diversity and economic aspects. One of the main focuses is the electrification of the Vehicle, and improvement of the battery system safety and performance.
http://www.eucar.be/publications/EUCAR%20FOCUS%202009_Web.pdf

[4] EUROLION – is a European R&D project aiming at developing a new Li-ion cell for traction applications. The wide spectra of activities include testing and benchmarking of formulated alternatives.
http://www.euroliion.eu/project-description/

[5] SuperLIB- "*Smart Battery Control System based on a Charge-equalization Circuit for an advanced Dual-Cell Battery for Electric Vehicles*" is a European project focusing on charge distribution control and thermal control to enhance the battery performance over its lifetime. A state of health model is built based on cell characterisation and testing.
http://www.superlib.eu/

[6] HELIOS-(High Energy Lithium IOn storage Solutions)
Evaluation of four Lithium battery packs of different chemistry in terms of electrical performance and safety through life cycle tests during normal and abusive test conditions. The aim is to improve the long-term visibility of the battery performance.
http://www.helios-eu.org/

[7] AMELIE- (Advanced Fluorinated Materials for High Safety, Energy and Calendar Life Li Ion Batteries) aims to develop a cell prototype for PHEV and EV applications. Testing of the cell performance is an important part of the activity.
http://amelie-green-car-project.fr/about/

[8] L. Borgarello, C.Ricci, H. Benzaoui, L. Berzi, "*Methodology to build vehicle "mission profile*": Combining different sources and application of the methodology on case studies", ASTERICS D1.4, 2014, unpublished.

[9] S. E. Li, B. Wang, H. Peng, X. Hu, "*An electrochemistry-based impedance model for lithium-ion batteries*," J. Power Sources, vol.258, pp.9-18, February 2014.

[10] B. Stiasznya, J.C. Ziegler, E.E. Krauß, M. Zhang, J.P. Schmidt, E. Ivers-Tiffée, "*Electrochemical characterization and post-mortem analysis of aged $LiMn_2O_4$-$Li(Ni_{0.5}Mn_{0.3}Co_{0.2})O_2$/graphite lithium ion batteries part I: Cycle aging*", Journal of Power Sources vol.251, pp.439-450 2014.

[11] B. Emmanuel, "*Constant phase elements, depressed arcs and analytic continuation: A critique*", Journal of Electroanalytical Chemistry 624 14–20, 2008